Prediction of growth of jet fuel autoxidative deposits at inner surface of a replicated jet engine burner feed arm

Alborzi, Ehsan; Blakey, Simon; Ghadbeigi, Hassan; Pinna, Christophe

DOI:
10.1016/j.fuel.2017.10.006

Document Version
Peer reviewed version

Citation for published version (Harvard):
Alborzi, E, Blakey, S, Ghadbeigi, H & Pinna, C 2018, 'Prediction of growth of jet fuel autoxidative deposits at inner surface of a replicated jet engine burner feed arm', *Fuel*, vol. 214, pp. 528-537.
https://doi.org/10.1016/j.fuel.2017.10.006

Prediction of Growth of Jet Fuel Autoxidative Deposits at Inner Surface of a Replicated Jet Engine Burner Feed Arm

Ehsan. Alborzi[1], Simon. Blakey, Hassan. Ghadbeigi, Christophe. Pinna

Department of Mechanical Engineering, The University of Sheffield, Sheffield, England

Abstract

A low thermally stable jet A-1 fuel was heated up to 115 hours under engine representative condition in a simulated burner feed arm with cylindrical shape using"Aviation Fuel Thermal Stability Test Unit (AFTSTU)". The local growth of surface carbonaceous deposits was measured by the use of three K-type thermocouples which were inserted in discrete locations along the inner surface of heated tube. Subsequenly, the deposited tube was sectioned and prepared for"Scanning Electron Microscopy(SEM)" to visualise the circumferential profile of the carbonaceous deposit. This helped to identify the axial profile of deposit thickness by integration of the average deposit thickness at five cross sections along the tube. Using the temperature rise data, a one dimensional, analytical heat transfer model was used to calculate local deposit thickness as a function of time.

A transient fuel dependent, two stage chemical kinetic model was developed to simulate the growth of deposit as a function of time, temperature, and fuel chemical composition. In this model, the growth of deposit was assumed to be equal as a geometrical displacement in radial direction. Such a displacement is explicitly calculated using an initial rate of deposition(steady state at t=0) and accelerating deposition rate(at $t = t + \Delta t$) to account for the non linear rate of deposition over the period of thermal exposure time. The concentration of insoluble species and initial rate of deposition as well as temperature at the adjacent layer to the heated surface were obtained through a steady state"computational fluid dynamics(CFD)" simulation using pseudo detailed mechanism of fuel autoxidation by Kuprowicz et.al[1]. The rate parameters of the accelerating deposition rate were optimised by the application of pattern search method with respect to the calculated de-

*Corresponding author

Email address: e.alborzi@sheffield.ac.uk (Ehsan. Alborzi)

posit thickness from one dimensional heat transfer model. Eventually, the optimised model was used with a transient CFD model with dynamic mesh using Ansys Fluent commercial package to simulate the growth of deposit in a reactive flow medium. The simulated results are in good agreement with the experimental data obtained from visualised deposit.

Keywords: `Aviation fuel, thermal oxidative stability, surface deposition`

Nomenclature

Δy	(Distance to the nearest wall)(m)
ϵ	Emissivity (W/m^2)
$\frac{d\delta}{dt}$	Initial rate of deposition $(kg/m^2.s)$
μ	(Dynamic viscosity)$(kg/m.s)$
ρ	Density of fluid (kg/m^3)
$\rho_{precursor}$	Density of insoluble materials (kg/m^3)
τ_w	(Wall shear stress) $(kg/m.s^2)$
$f_{precursor}$	Precursor mass fraction in the first row of computational cell in heated wall adjacency
J_k	Effective diffusivity of species k (m^2/s)
M_W	Molecular weight of insoluble (kg/mol)
Q	Heat flux (W/m^2)
Sd_k	Chemical source term for consumption of species k
Sf_k	Chemical source term for formation of species k
$[\frac{d\delta}{dt}]_{t+\Delta t}$	Cumulative rate of deposition $(kg/m^2.s)$
$\Delta\delta$	Deposit thickness (m)
δP	Penetration depth (m)
μ_m	Magnetic permeability of stainless steel (H/m)
ρ_D	Density of deposit (kg/m^3)
ρ_R	Resistivity of stainless steel (Ωm)
σ	Stefan-Boltzmann constant$(W/m^{-2}k^{-4})$

A_1	Pre exponential factor for initial deposition stage(s^{-1})
A_2	Pre exponential factor for transient deposition stage (s^{-1})
E_{a1}	Activation energy for initial deposition stage ($kcal/mol$)
E_{a2}	Activation energy for transient deposition stage ($kcal/mol$)
f_i	Frequency of induction (kHz)
h_{fuel}	Natural convection heat transfer for fuel ($W/m^2.K$)
n	Surface factor (dimensionless)
R	Universal gas constant ($J/molK$)
r	Updated radial position (m)
r_0	Initial radial position (m)
T	Absolute temperature (K)
T_0	Wall temperature at time zero (K)
T_a	Air temperature (K)
T_t	wall temperature at time t (K)
T_w	Wall temperature (K)
T_{bulk}	Bulk fuel temperature (K)
y^+	Distance from the inner wall to the nearest node (dimensionless)

1. Introduction

Gas turbine fuels are exposed to thermal stress on route from the fuel tank through the engine to the combustion chamber. Due to the heat transfer from engine components to bulk fuel, the fuel temperature increases. In such a situation fuel begins to degrade which manifests itself by formation of a series of soluble and insoluble products. These products collectively participate to the formation of surface carbonaceous deposits in fuel system. Within jet fuel system, burner feed arms are at the highest risk of deposition.

A robust theoretical framework allows the prediction and control of deposit build up so that feed arms may be designed with an acceptable maintenance frequency and life span. Several studies conducted on jet fuel thermal degradation over the past few decades have attempted to provide quantitative information on the impact of operating variables on surface deposition.

However, given a large number of interacting parameters, many tests are needed to isolate the individual effects and hence a comprehensive predictive model for practical application is still lacking.

As an alternative solution, application of empirical models is useful approach where complex small scale events occurring at fuel-surface interface are solved by small number of equations with physically reasonable forms. The robustness of such models is primarily dependent on the similitude of the experiment with realistic conditions met in aero engines as the model parameters need to be calibrated based on the experimental results. It is noteworthy that due to the fuel volume and test time required, a representative test at full scale is remarkably costly; therefore there are always compromises between the number of controlling parameters and test conditions based on the goal of the research and available resources. The AFTSTU[2]-[3]-[4] is a pilot scale test rig capable of assessing interactions of a simulated aero engine fuel system with fuel thermal degradation. This rig replicates conditions in a range of current and future aero engines ensuring that the fuel arrives at the simulated burner feed arm in a fairly representative condition to that in service.

The work presented here describes a new transient fuel dependent, two stage kinetic, empirical model for jet fuel autoxidative surface deposition. This model was implemented into a two dimensional axis symmetric CFD case file created in Ansys Fluent with a moving boundary corresponding to the fuel wetted surface along the heated tube. It was assumed that the boundary displacement is the net result of transformation of all insoluble materials generated in heated surface adjacency into the deposit layer. This is according to the assumption made by Moses[5] that when the temperature at fuel wetted surface is at least 45 °C higher than core temperature, almost 90% of the insoluble materials will be formed within the laminar sublayer.[6] This assumption is based on the fact that approximately two thirds of temperature changes occur within the laminar sub layer and that the formation of deposit precursors follows an exponential relation to the bulk fuel temperature. The AFTSTU was used for the experimental study of autoxidative deposit build up in a simulated burner feed arm. Pattern search optimisation technique was used outside the CFD calculation to calibrate the model parameters with respect to the experimental data obtained from the AFTSTU. Contrary to the previous transient deposition models such as Krazinski et.al[7], Roquemore and Reddy[8] and Katta and Roquemore[9], the empirical model presented here employs more realistic autoxidation chemical kinetic mechanism for conventional jet fuel as presented in references[10],[11],[12] and[1].

2. Experimental Work

2.1. Jet Fuel Thermal Stressing Test

The feed arm represents a cold drawn 316 stainless steel, cylindrical tube with 6 mm od and 2 mm id. This contains a series of 6 K-type sheathed thermocouples silver brazed into the tube wall. The thermocouples were arranged in two sets of three and inserted in the locations 2(Thermocouple A), 3(Thermocouple B) and 4(Thermocouple C) as shown in figure1. The three outer thermocouples are 0.2 mm from the tube outer surface and the three inner are 0.4 mm from the inner tube surface respectively. A radio frequency induction coil with a total length of 120 mm was centered on the second axial thermocouple (point 3 in figure1). The fundamental principle of the induction heating is based on the electromagnetic induction, where the current is induced in the conductive materials and as a result of the electrical resistance, heat is generated in the material. The electromagnetic field penetrates to a certain depth from the surface of the material, known as the skin effect[13]. The skin effect is explicitly described in the numerical section of this work. The simplified schematic of the AFTSTU is shown in figure2.

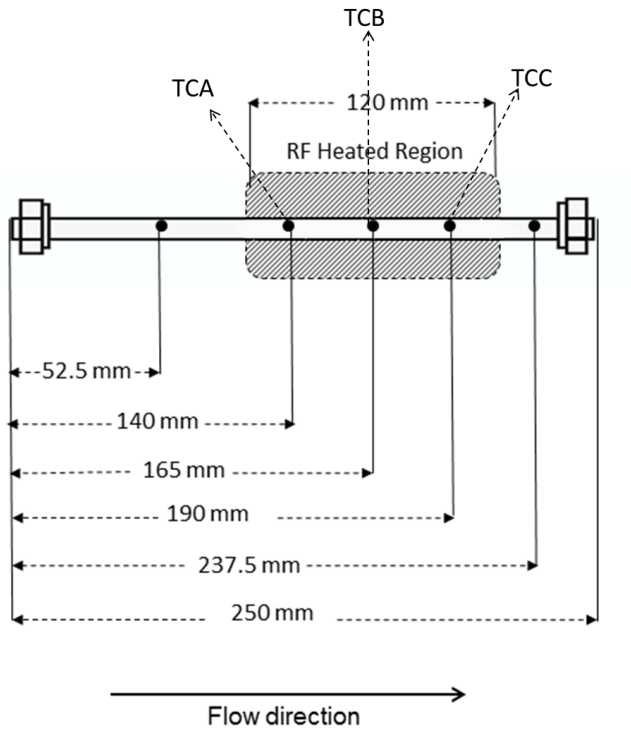

Figure 1: Cutting cross sections along the heated tube(not to scale)

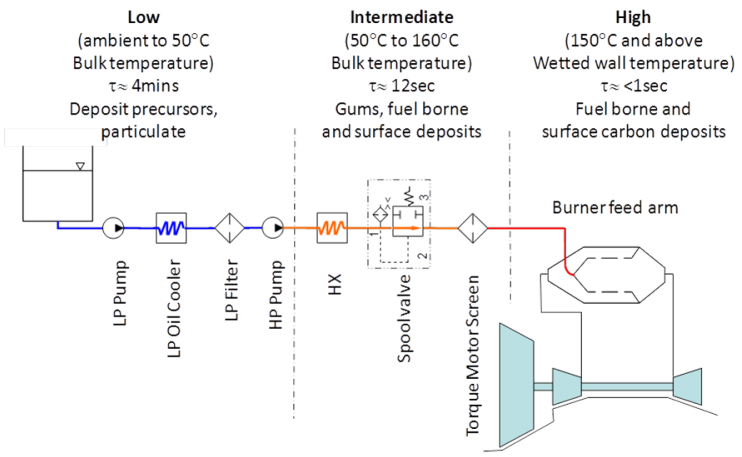

Figure 2: The simplified schematic of the AFTSTU showing its different thermal regimes

The fuel sample was analysed externally using an in house method as developed by Intertek. This method determines sulfur containing compounds and group types in middle distillates using an Agilent 7890 N"Gas Chromatograph(GC)" equipped with a Zoex thermal modulation and an Agilent 355 sulfur chemiluminescence detector. Quantification of sulfur classes was carried out by the normalisation to the total sulfur content as determined by combustion followed by UV-Fluorescence. The $GC \times GC$ analysis separated sulfur-containing compounds according to their boiling point and upon their polarity. Thus it was possible to elute the benzothiophenes and dibenzothiophenes in two well-defined bands clearly separated from the band of thiophenes, sulfides and mercaptans. Hydrocarbon speciation was carried out using "UOP Method 990-11'. This method determines molecular type homologous series by carbon number.

It was assumed that the concentration of dissolved oxygen in the jet fuel is approximately 70 ppm in line with the references[14, 10, 11, 12, 1].

Chemical species	Concentration	Methods
n-Praffins	20.67% m/m	$GC\ X\ GC - FID(UOP\ 990 - 11)$
iso-Praffins	24.77% m/m	$GC\ X\ GC - FID(UOP\ 990 - 11)$
Cyclics	30.84% m/m	$GC\ X\ GC - FID(UOP\ 990 - 11)$
Alkylbenzenes	16.18% m/m	$GC\ X\ GC - FID(UOP\ 990 - 11)$
Indans and tetralins	2.15% m/m	$GC\ X\ GC - FID(UOP\ 990 - 11)$
Naphtalenes	1.33% m/m	$GC\ X\ GC - FID(UOP\ 990 - 11)$
Antioxidant	25 mg/l	$GC\ X\ GC - FID(UOP\ 990 - 11)$
Thiols, Sulfides and Disulfides	310 mg/Kg	$GC\ X\ GC - SCD$
Total Hydroperoxides	7.8 μM	West et.al [15]
JFTOT	260 °C	$D3241/IP323$
Distillation		$D86/IP123$
IBP	149.8 °C	
10 % recovered	168.9 °C	
20 % recovered	178.2 °C	
50 % recovered	197.0 °C	
90 % recovered	239.2 °C	
FBP	262.2 °C	
Density	801 kg/m^3	$D4052/IP365$

Table 1: Composition of major hydrocarbon and some of the heteroatomic species quantified in tested fuel

Prior to the thermal exposure test, the feed arm was treated with a mixture of weak hydrofluoric and nitric acids solutions to clean the internal surface of the tubes to achieve a repeatable surface finish. The feed arm was initially heated to a predetermined temperature. During this phase the temperature was controlled at the inner wall by the second thermocouple(third point in figure1). During the test, fuel entered the nozzle section at approximately 175 °C following conditioning in the upstream sections of the rig. It then flowed past the hot wetted wall surface of the nozzle and out to the rest of the rig. We observed that for a given inductive power, the temperature distribution along the wall were in the range of 250 °C to 270 °C. By wall we refer a a line passing through the thermocouples's tips which is 0.4 mm distant from the tube inner wall. Corresponding to this temperature range, the fuel temperature between inlet and outlet increased by approximately 16 °C. Therefore, once steady state heat transfer was achieved the heating power was fixed for the corresponding temperature. The test conditions used in the AFTSTU are presented in table 2.

Test Parameters	**Values**
Flow Rate(l/h)	23
Pressure in low pressure section in (psi)	50
Bulk temperature in low pressure section in (°C)	50
Pressure in high pressure section in (psi)	500
Bulk temperature in high pressure section in (°C)	175
Test Duration(h)	115
Initial Wall temperature prior to test(°C)	25
Residence time in tube centre line(s)	0.159

Table 2: Test conditions in AFTSTU

Once the test was complete, it was possible to apply a number of approaches to further study the deposit formed on the inner surfaces of simulated burner feed arm. These approaches include: carbon burn off for quantification of total deposit mass, gravimetric method for total mass of deposit and tube sectioning and measurement of deposit thickness at discrete axial locations. The application of carbon burn off and gravimetric method will give only one results corresponding to the total mass of deposit without proving extra information about the deposit profile and its morphology. In this work only tube sectioning and SEM microscopy was used for deposit visualisation and model validation.

2.2. Deposit Thickness Measurement

Given the large size of the feed arm, small specimens from 5 locations along the deposited tube were sectioned for microscopy. The cutting points are indicated in figure1. The first section corresponds to a halfway point between the nozzle inlet and the beginning of thermal exposure region and sections2, 3 and 4 match up with the axial locations of first, second and third thermocouples. Section5 is halfway between the end of thermal exposure region and the nozzle exit.

The cutting method and associated cutting parameters are crucially important to maintain the initial structure of the deposited layer. For this reason, the Buehler Isomet precision cutting machine with diamond wafering blades was used to cut the specimen with a cutting speed of 2 mm/min. In order to minimise the risk of deposits structural changes during the cutting operation by heating, water based cutting fluid was used. The sections were subsequently cold mounted in a standard cylindrical mould using epoxy resin followed by the vacuum impregnation. The resin was left to cure for about 9-12 hours to obtain solid resin moulds containing the tube sections. The

vacuum impregnation is to ensure that no air was left in the mounted specimen and the resin had completely filled up the porous structure of the deposit. The mounted specimens were then mechanically polished to obtain flat, scratch free surfaces that enable cross section analysis of the deposited tube. The mechanical polishing started using abrasive papers and very fine polishing 1 µm diamond paste was used in the final polishing step to achieve a mirror polish surface for the specimen. The specimens were washed thoroughly with water and dried with a hot air blow after each polishing step to avoid surface contamination. The polished cross sections were firstly investigated using optical light microscopy. The main drawback of the optical light microscopy is the visible lights in the imaging processing that reduce the achievable resolution and the depth of field by the wavelength of the applied light. As an alternative solution, SEM was used to achieve higher magnification and a better resolution. It is noteworthy that the surface of the cut samples were checked using optical microscopes in order to ensure the deposit mass is maintained at the cut section. This would be evident from the surface topography of the samples since any lost deposit material will result in micro cavity formation at the surface that can be observed using optical and SEM microscopes. Although there might be the risk for more brittle deposit formed at the latest stage to be washed off during the preparation stage. It is noteworthy to mention that as the inner surface is not smooth and have cracks and fissures the deposit profile in radial direction presents some variations.

3. Numerical Method

In this work, it was assumed that the bulk fuel autoxidative reactions remain unchanged over the course of surface deposition and that the 100 % of insoluble materials transform to deposit layer. This is however a weak assumption and in practice some of the insoluble reaching the heated wall bounce back to the fuel in heated wall adjacency region. Ervin et.al[16] employed a sticking probability function in a time dependent CFD simulation for calculation of deposit growth in a near isothermal flowing tube reactor. The sticking probability is expressed as the likelihood that a particle reaching the heated wall remain there and includes an Arrhenius-like dependence on the wall temperature.

The density and thermal conductivity of of depositing materials in this work is assumed constant. The authors are well aware of the fact that this is also not a true assumption and the density of depositing materials changes over

the course of the surface deposition. Our assumption was made to simplify a sequence of very complex physico-chemical interactions. There are evidences that the deposition at early stage is dominated by the interactions between the active sites of the heated surface including Ni and Cr, O_2 and S. The C−C interactions will become dominant in the middle stage of deposition.[17] More fundamental research is required to explore the underlying of deposition from the early stage to be able to explain various distinctive phases of deposition including induction period, accelerating zone and level off region. This is outside of the scope of our work and for the simplicity it has been assumed that depositing materials is homogeneous with the property of carbon.

A steady state, two dimensional axis symmetric CFD simulation was performed to identify the temperature distribution along the intact fuel wetted surface. Local concentration of insoluble species(deposit precursor) at heated wall adjacency layer was obtained by the numerical solution of diffusion equation and the relevant chemical source terms were calculated through the integration of pseudo detailed chemical kinetic mechanism of Kuprowicz[1]. For steady state simulation, the computational domain was divided into three sub domains corresponding to the stainless steel, RF skin depth, and bulk fuel and all were meshed with structured pattern composed of rectangular cells. The full resolution of numerical boundary layer and the associated laminar sublayer are essential for the accuracy of heat transfer between intact heated tube and wall adjacency layer in bulk fuel. Therefore the standard $k-\epsilon$ turbulent model with enhanced wall function[18] was used. The dimensionless distance from the inner wall to the nearest node was restricted to $y^+ < 5$ in line with the accepted practice as illustrated in equation 1. This resulted in a very fine grid structure with first grid line at 0.025 mm normal to the wall.

$$y^+ = \frac{\rho \Delta y}{\mu} \sqrt{\frac{\tau_w}{\rho}} \tag{1}$$

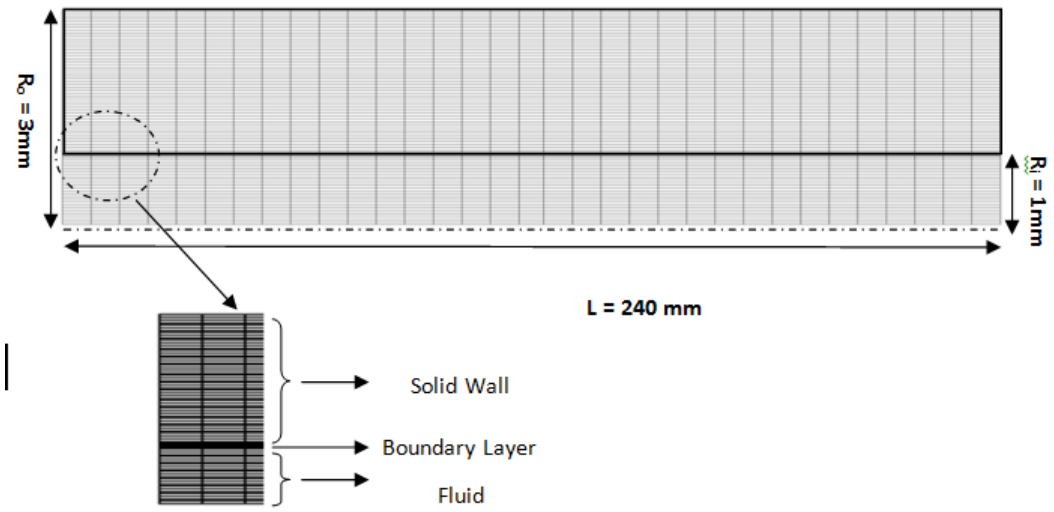

Figure 3: Mesh geometry and grid pattern for replicated feed arm burner, enlarged in y direction

Thermal properties of aviation fuel including density, specific heat, viscosity and thermal conductivity were considered as temperature dependent functions which were built and used in the form of user defined functions in Fluent according to data presented in CRC Aviation Handbook[19]. Thermal properties of the stainless steel were assumed constant and taken from material data base in Ansys Fluent. The properties of the air surrounding the outer tube wall surface were based on the data from literature[20].

A mean inlet velocity equal to 1.57 m/s at a constant temperature of 175 selsius was considered for the inlet boundary at a location $> 12D$ prior to the physical inlet. In practice, both velocity and temperature become fully developed prior to the physical fuel inlet. At this condition, the Reynolds number was approximately equal to 10000. The tube exit was defined as an outflow boundary condition due to the unknown velocity and pressure field at this location. For all outer wall boundaries of the model, heat flux was specified as illustrated in equation2.[20].

$$Q = h(T_a - T_w) + \epsilon\sigma(T_a^4 - T_w^4) \tag{2}$$

Where ϵ denotes the external emissivity and its value for most types of stainless steel is 0.4, T_a signifies the free stream temperature, T_w represents the tube wall temperature which was unknown. The external natural convection heat transfer coefficient was calculated to be 13.94 $\mathrm{W/m^2K}$. The inner tube surface was defined by a coupled wall boundary condition and no slip condition was chosen. An internal energy generation source term was used to

replicate the RF heating generated by the induction coil. The penetration depth was calculated by the equation3.[13]

$$\delta P = \sqrt{\frac{\rho_R}{\pi \mu_m f_i}} \tag{3}$$

Where ρ_R is the resistivity of the stainless steel equal to 47.8×10^{-8} Ωm, μ_m represents magnetic permeability of the stainless steel equals to 1.256×10^{-4} H/m and f_i denotes the frequency of induction equals to 284 kHz. Therefore, penetration depth was 0.6 mm from the outer tube wall. This was implemented in Ansys Fluent as a user defined function to include the skin effect.

The coupling of chemistry and flow equations is described in equation4. This equation illustrates the formation, consumption and transportation of a given species k within the thermally stressed jet fuel. The rates of formation and consumption of chemical species was calculated by the integration of ordinary differential equations representing the pseudo detailed mechanism of fuel autoxidation. The transport of chemical species was assumed to be according to the transport of diluted species. This assumption is well justified considering the concentration of chemical species contributing to the autoxidative reactions is small compared to the bulk fuel. The laminar diffusivity of all species in this work is assumed to be constant at a value of $10 \times 10^{-8}\,\mathrm{m}^2/$sexcept for insoluble species which is set as $10 \times 10^{-12}\,\mathrm{m}^2/$s.[21]

$$\frac{\partial(k)}{\partial t} + \frac{\partial(\rho U_i k)}{\partial x_i} = \frac{\partial}{\partial x_i}\left(J_k \frac{\partial k}{\partial x_i}\right) + Sf_k + Sd_k \tag{4}$$

Where ρ is the density of bulk fuel, k denotes the concentration of any chemical species involved in bulk fuel autoxidation mechanism, U_i represents the local velocity in x direction, J_k is the effective diffusivity of the k, Sf_k and Sd_k are the source terms representing the generation and consumption of species k per unit volume.

3.1. Simulation of Time Dependent Growth of Deposit

A geometry composed of three computational regions including solid(stainless steel), fluid(bulk fuel) and a virtual layer within the tube boundary layer was created as shown in figure 4. The virtual layer has no physical sense and was created to allow initialising the cumulative deposits build up using a transient model of surface deposition as described below. This model was applied

as user defined function to the boundary of the virtual layer bordering the computational domain corresponding to the bulk fuel.

The two stage kinetic transient model is described in equations 5,6,7,8,9 and 10. The model illustrates an explicit method of calculation for cumulative surface deposition rate. The method for time dependent deposition modelling in this paper is partly based on works published by Ervin et.al[16], Katta et.al[9] and Roquemore and Reddy[8]. We introduced an additional equation which illustrates the cumulative rate of deposition purely based on previous experimental results of various types of aviation fuel obtained in our lab.

The calculation initiates from a steady state rate at time(t=0) as illustrated in equation 5 where $\rho_{precursor}$ denotes the density of precursor species in kg/m^3, $f_{precursor}$ represents the mass fraction of precursor species at the first row of computational cell in heated wall adjacency, $MW_{precursor}$ is the molecular weight of deposit precursor species and k_1 is the rate constant. The temperature dependency of the rate coefficient is expressed by an Arrhenius equation as shown in equation6.

The time dependent, one dimensional equation9 was introduced to simulate the non-linear behaviour of surface deposition over the period of thermal exposure. In this equation the cumulative deposit build up was approximated as a geometrical displacement($\Delta\delta$) from an initial radial position of the intact surface (r_0) to an updated position(r) at ($t+\Delta t$). The updated position was coupled with the cumulative rate at ($t+\Delta t$), time step(Δt), (r_0) and density of carbon deposit(ρ_D). We introduced an exponent n as a surface factor which depends on the molecular interactions between fuel chemical compositions and surface constituents at various stage of deposition. Further fundamental research is needed to expand the surface exponent which is beyond the scope of this work. The temperature dependency of the cumulative rate is explained by equation10. For simplicity, thermal properties of the deposit layer were assumed as constant over time and sticking probability was not considered herein. The pattern search optimisation method, as developed by Hooke and Jeeves[22] was used to optimise the kinetic parameters and the The exponent n.

$$\left[\frac{d\delta}{dt}\right]_{t=0} = k_1\left[\frac{\rho_{precursor} f_{precursor}}{MW_{precursor}}\right] \tag{5}$$

$$k_1 = A_1 e^{(\frac{-E_{a1}}{RT})} \tag{6}$$

$$\Delta\delta = r - r_0 \tag{7}$$

$$r = r_0 \sqrt{1 - \frac{2\frac{d\delta}{dt}_{t+\Delta t}\Delta t}{\rho_D r_0}} \tag{8}$$

$$\left[\frac{d\delta}{dt}\right]_{t+\Delta t} = k_2 \left[\frac{\Delta\delta}{r_0}\right]^n \tag{9}$$

$$k_2 = A_2 e^{(\frac{-E_{a2}}{RT})} \tag{10}$$

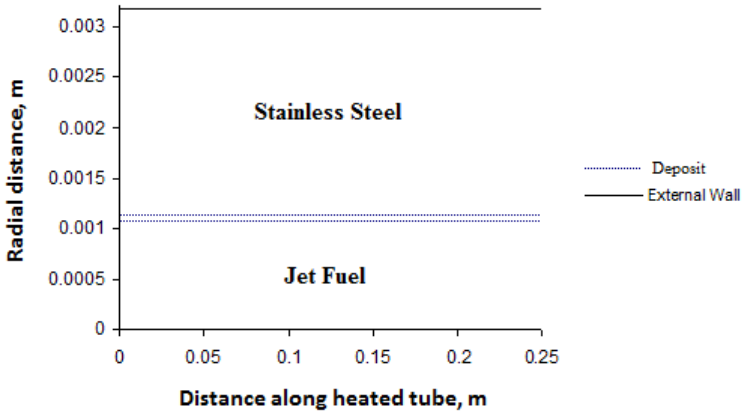

Figure 4: The schematic of computational domain including solid and liquid regions and a virtual layer for growing deposit. This figure is enlarged in radial direction

4. Results and Discussion

4.1. Fuel Thermal Exposure Test Results

The values measured by the thermocouples A, B and C indicate that the temperature at the outer surface of the simulated burner feed arm increased over the course of thermal exposure experiment as shown in figure 5. The temperature rise is attributed to the thermal insulation characteristics of depositing materials. Given that the depositing materials primarily consist of carbonaceous materials, the ability of deposits to conduct thermal energy is significantly lower than the stainless steel. Therefore, while the heating generated by the RF heater was constant throughout the experiment, the

temperature at the outter surface of tube increased.

Previous studies using different types of aviation fuels in the AFTSTU indicate that the temperature rise along the simulated burner feed arm is manifested by three distinctive regions including an induction period through which no or negligible deposit forms, a substantial rise followed by a level off region where deposit formation settles down. The length of the induction period as well as the slope of temperature rise in the second region is specific to the fuel type and the location along the heated tube. In contrast, the same typical behaviour was not observed in this experiment. This is likely to be due to the low thermal stability of the jet fuel used in this work. This was justified by the relatively high concentration of sulfides and hydroperoxides in the fuel. Therefore, an accelerating surface deposition from the beginning of thermal exposure was observed.

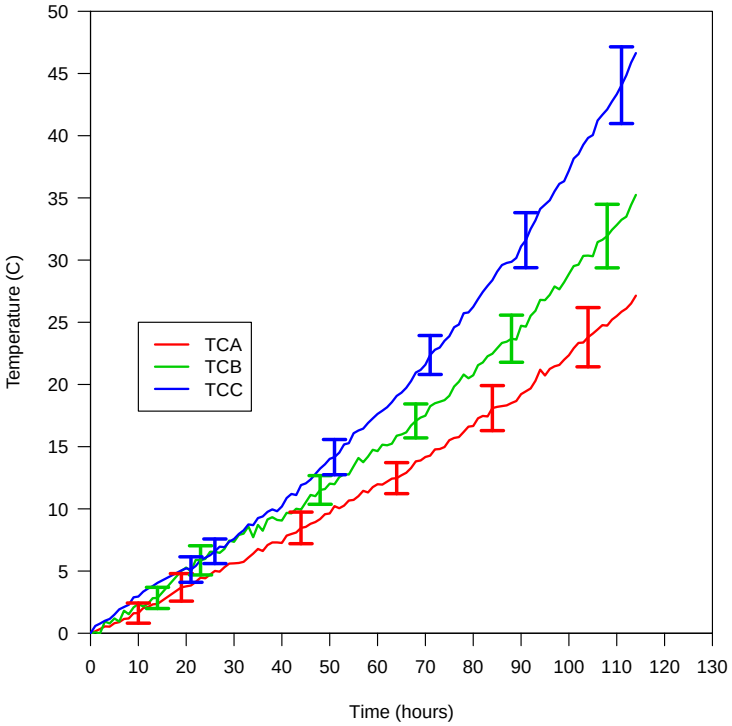

Figure 5: Wall temperature rise due to surface deposition as recorded by thermocouples A and B and C

4.2. Investigation of Deposit Thickness at Circumferential Positions

Due to relatively large size of the cross sections of the simulated burner feed arm, a low magnification image was taken to indicate the orientation of the specimen in the SEM chamber as shown in figure 6. Construction of an elongated field of view such as a fully 360° image of deposit at each cross section is a laborious task since only small portions of plane were visible at higher magnified images. For this reason, the SEM analysis was carried out at only four circumferential positions separated by 90° for each cross section. We considered 0° angle as a starting point for the analysis as this position corresponds to the location of the thermocouples' tips the regions where the experimental data were obtained.

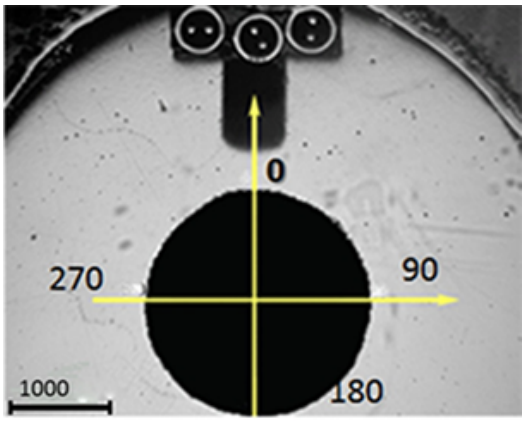

Figure 6: Cross section of the AFTSTU heated nozzle representing various angles for SEM analysis

The images taken by SEM at section1 revealed that the thickness of deposited layer at this plane is negligible. This indicates that the increase of temperature at fuel wetted surfaces for the regions prior to the induction heating unit is not high enough to initiate thermal degradation reactions for the fuel tested. A series of magnified pictures at other four cross sections along the AFTSTU heated nozzle are shown in figure 7. It was observed that at cross section2 deposit profile is rather inconsistent and varied from one point to the next and at some regions the tube internal surface were also intact. At this cross section, in circumferential direction, the average deposit thickness varies from approximately 5 μm at 0° to a maximum value of around 7 μm at 90° then decreased to about 6.5 μm at 180°and remained more or less the same for 270°.

Comparison of the images at cross sections3 and 4 and linking these to the results shown in figure 5 indicates that the surface deposition increased substantially from cross section3 to 4. At cross section3, the average deposit thickness was in the order of 10 μm at 0° circumferential position and fell to approximately 8 μm at 90° and 180° then increased to about 10 μm at 270°. A surface defect with a depth of around 5 μm was found in the image corresponding to 180° at cross section3. The defect starts from the internal surface and penetrates deep into the tube wall. It appears that surface deposition decelerated from cross section4 to 5. Furthermore, the average deposit thickness varied from approximately 4.5 μm at 0° to around 6.5 μm at 90°. It was observed that deposit thickness is irregular at cross section5 from one point to the next; although, the patches from fresh tube were fully covered by a thin deposit layer.

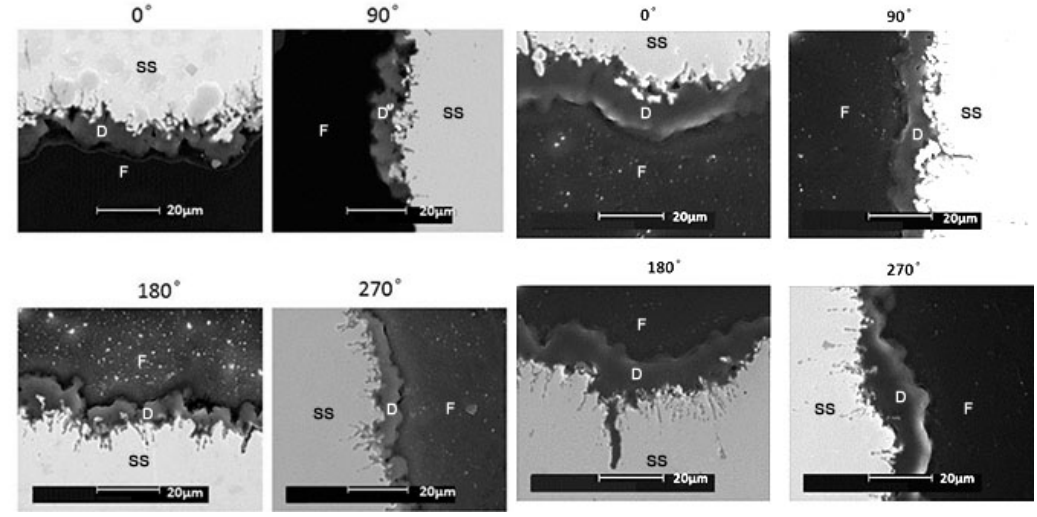

(a) Cross section2

(b) Cross section3

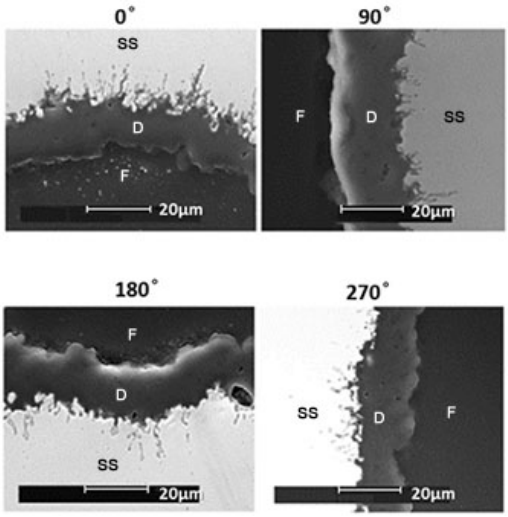

(c) Cross section4

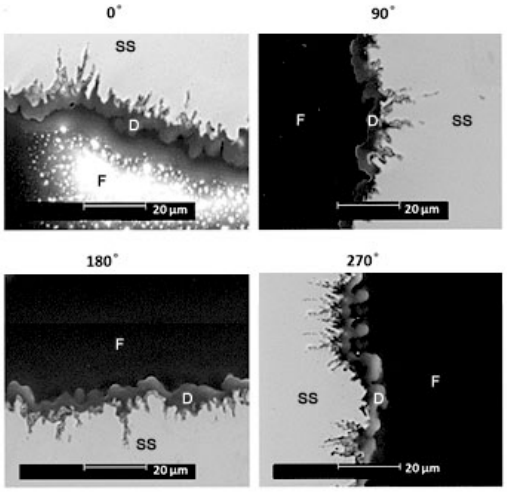

(d) Cross section5

Figure 7: SEM images of stainless steel, deposit layer and fuel passage at 4 cross sections along the AFTSTU heated nozzle for different angles. SS, D and F signify stainelss steel, deposit layer and fuel passage respectively.

4.3. Model validation

The temperature rise data were used to calculate the local deposit thickness at thermocouples' tips using a one dimensional heat transfer model as described in equations 11 and 12. It was assumed that the heat flux through the wall of the tube is constant given that the bulk fuel temperature rise

throughout the testing is constant.

$$\frac{T_0 - T_{bulk}}{\frac{1}{h_{fuel}}} = \frac{T_t - T_{bulk}}{\frac{1}{h_{fuel}} + \frac{\delta_t}{k}} \tag{11}$$

Where T_0 is the wall temperature at time zero and T_t represents the wall temperature at time t. δ_t is the deposit thickness at time t, h denotes the convective heat transfer coefficient and k represents thermal conductivity of deposited materials. Therefore the calculation of deposit thickness can be reduced to a function of the change in wall temperature, $T_t - T_0$:

$$\delta_t = a\frac{k(T_t - T_0)}{h(T_0 - T_{bulk})} \tag{12}$$

Where a is an empirical correction factor based on previous experimental data to account for the morphology of the deposit layer. A number of studies have investigated the conductivity of typical deposits found in aviation fuel autoxidation test rigs of a range of scales. TeVelde and Glickstien [23] reported a strong variation in deposit conductivity with deposit thickness between 20 µm and 25 µm varying by an order of magnitude from $0.017W/m^2K$ to $0.17W/m^2K$. Earlier experimental work on sectioned tubes from the AFTSTU [4] has suggested an estimated thermal conductivity of to $0.012W/m^2K$ would be appropriate and was validated against microscope assessment of sectioned tubes from the rig. This agrees well with the work of Tevelde and Glickstein as the deposit was below 20 µm for the majority of the testing work. The bulk fuel temperature was estimated from the bulk fuel temperature data, and a local value of heat transfer coefficient, h, was obtained from the steady state CFD simulation.

Subsequently, kinetic parameters of the transient model were optimised with respect to the calculated local deposit thickness using one dimensional heat transfer model. As to initialise the constrained optimisation process, for each parameter, an initial value and a range of values were required as shown in table 3. Due to the unbeknownst interactions amongst the surface constituents and bulk fuel chemical species, this range was selected arbitrarily with no physical sense. Further comprehensive research at molecular level is required to explicitly define and expand the kinetics of surface-liquid phase interactions over the course of surface deposition.The results of optimized deposit thickness and one dimensional calculated deposit thickness are presented in figures 8a, 8b and 8c.

Parameter	Initial Guess	Optimized Value	Lower Limit	Lower Limit
n(rate exponent)	0.001	0.075	0.00009	0.99999
Ea_1	5	15	1	20
A_1	1E1	1E3	1	20
Ea_2	5	15	1	20
A_2	1E1	1E3	1E0	1E9

Table 3: The initial guess and optimized values for the parameters

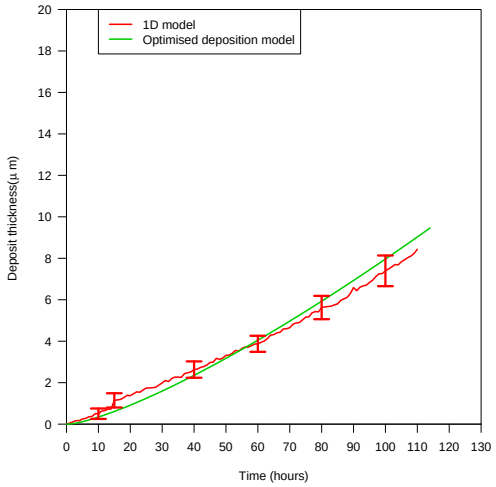

(a) Thermocouple A

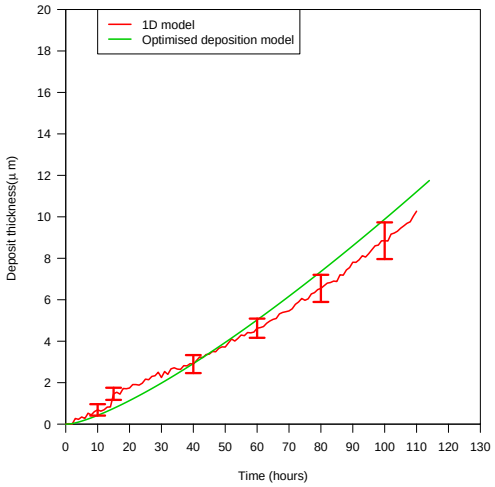

(b) Thermocouple B

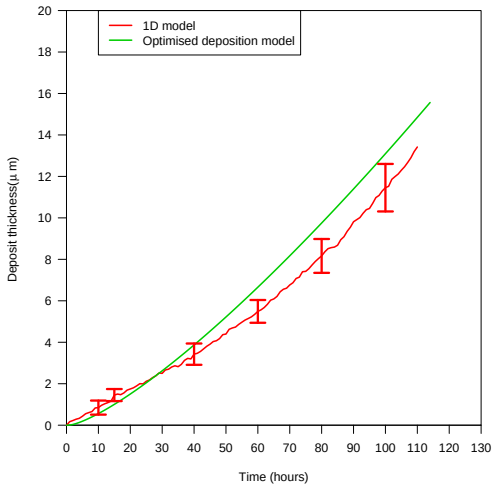

(c) Thermocouple C

Figure 8: Calculated cumulative deposit results at certain locations corresponding to the thermocouples' tips using optimised kinetic parameters and comparison with calculated deposit thickness obtained from one dimensional heat transfer calculation

The optimised transient model was used as a UDF with dynamic mesh and implemented to the fuel wetted boundary of the sandwich layer as shown in figure 4. The modeling results are in good agreement with average deposit thickness along the heated nozzle as shown in figure 9a. It can be seen that the peak of deposit thickness occurred in an axial distance of 195 mm irrespective of the circumferential positions however the calculated peak of deposit corresponded to nearly 210 mm. Such a discrepancy is due to the limited cross sections for SEM analysis. The transient model was used to calculate the amount of tube blockage as a function of thermal exposure time as presented in figure 9b.

The results of sensitivity of simulated deposit thickness to the initial values of dissolved oxygen are shown in figure 10a. As it is expected the decrease in the concentration of dissolved oxygen results in the drop of total surface deposit. This is evident as the local concentration of insoluble species at fuel wetted surfaces depends on the concentration of initial oxygen.

The simulated wall temperature rise as a result of deposit formation is presented in figure 10b. The sensitivity of temperature rise profile to the deposit's thermal conductivity is also shown. It can be observed that wall temperature rise is inverse proportional to the thermal conductivity of deposit. This means the lower value of thermal conductivity results in more insulative characteristics of deposit layer. Hence once the heat generation through the RF heater is constant the wall temperature increases.
With respect to the maximum thickness of deposit formed in tube, the fuel velocity is not violated as 25 μ is significantly shorter than the hight boundary layer.

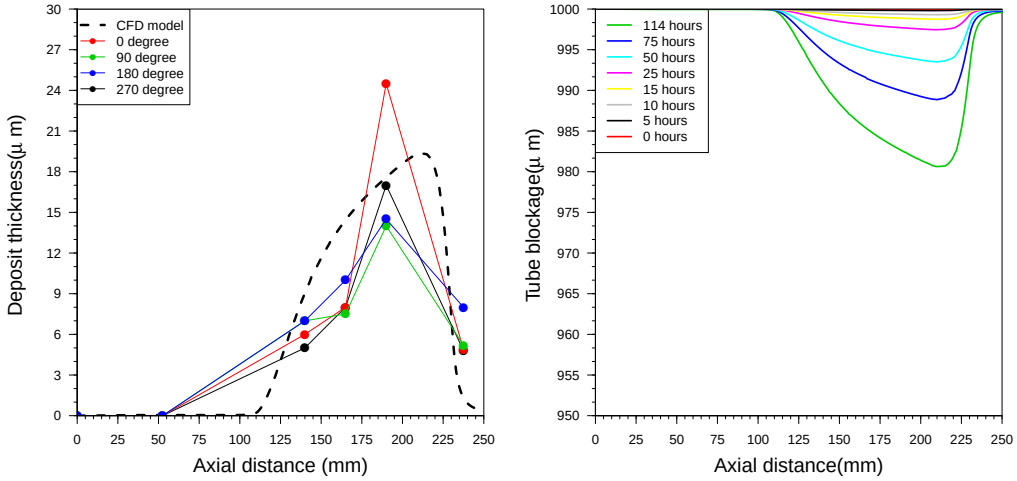

(a) Validation of model used with CFD

(b) Calculated amount of burner feed arm blockage employing model used with CFD

Figure 9: figure 9a presents validation of transient model of deposit growth implemented to CFD. Figure 9b indicates the amount of burner feed arm blockage as a function of thermal exposure time using transient model of deposit growth implemented to CFD

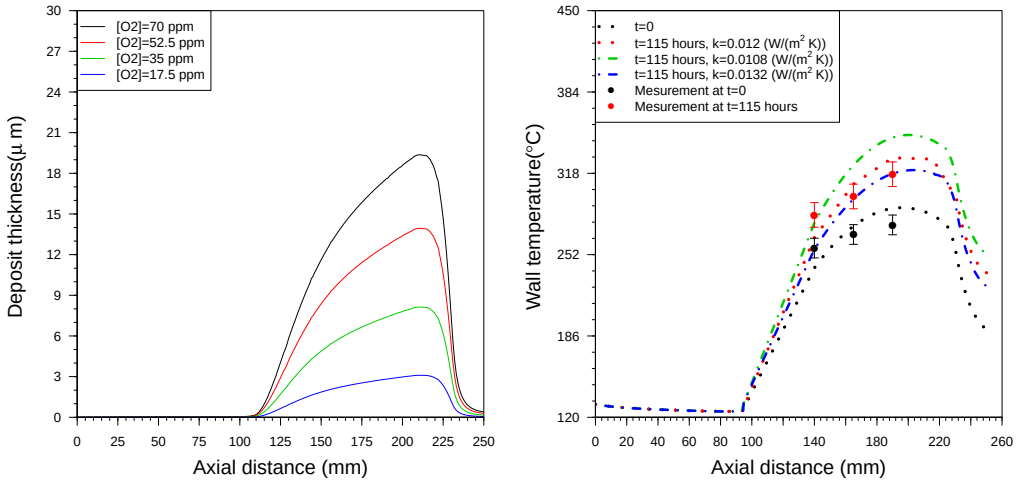

(a)

(b)

Figure 10: figure 10a presents the sensitivity of simulated deposit thickness on the initial values of dissolved oxygen. Figure 10b illustrates the simulated temperature rise along the wall at $t = 0$ and at $t = 115 hours$. Also the sensitivity of wall temperature rise on deposit thermal conductivity is presented.

5. Conclusion

- A low thermally stable Jet A fuel was thermally stressed in a simulated burner feed arm in an aero engine representative condition provided by the "Aviation Fuel Thermal Stability Test Unit (AFTSTU)" for up to 115 hours

- The formation of surface carbonaceous deposits was assessed indirectly by means of temperature measurements at the outter surface of the simulated burner feed arm.

- The deposited tube was sectioned and prepared for "Scanning Electron Microscopy(SEM)" to visualise the circumferential profile of the deposit. The SEM images show that deposit thickness varies both circumferential and axially. By integrating the average deposit thickness of the five cross sections, the axial profile of deposit along the burner feed arm was identified.

- An average value of thermal conductivity for carbonaceous deposit was used in a one dimensional, analytical heat transfer model for calculation of local deposit thickness as a function of time using the temperature rise data. The results of one dimensional heat transfer model showed good agreement with the temperature rise data.

- A fuel dependent, two stage kinetic model was developed and optimised with respect to the analytical heat transfer model using Pattern Search optimisation method. Subsequently, the optimised model was used with a transient "Computational Fluid Dynamics(CFD)" with dynamic mesh using Ansys Fluent commercial package to simulate the growth of deposit along the heated tube. The simulated results are in good agreement with the experimental data of visualised deposit.

- It was shown that the decrease in the concentration of dissolved oxygen results in the drop of total surface deposit. This is evident as the local concentration of insoluble species at fuel wetted surfaces depends on the concentration of initial oxygen.

- It was presented that wall temperature rise is inverse proportional to the thermal conductivity of deposit. This means the lower value of thermal conductivity results in more insulative characteristics of deposit layer. Hence once the heat generation through the RF heater is constant the wall temperature increases.

Acknowledgment

The assistance of Rolls-Royce for contributing rig test data is gratefully acknowledged.

References

[1] N. J. Kuprowicz, S. Zabarnick, Z. J. West, J. S. Ervin, T. Edwards, Use of Measured Species Class Concentrations With Chemical Kinetic Modelling for the Prediction of Autoxidation and Deposition of Jet Fuels, Energy & Fuels 21 (2007) 530–544.

[2] D. L. Dagget, A. Veninger, C. Lewis, R. Bullock, S.and Kamin, The Development of an Aviation Fuel Thermal Stability Test Unit, Journal of Engineering for Gas Turbines and Power 117 (1995) 468–473.

[3] S. Siouris, S. Blakey, C. W. Wilson, Investigation of deposition in aviation gas turbine fuel nozzles by coupling of experimental data and heat transfer calculations, Fuel 106 (2013) 79–87. doi:10.1016/j.fuel.2012.12.006.

[4] E. Alborzi, S. Blakey, H. Ghadbeigi, C. Pinna, C. Lewis, Investigation of surface deposition in a simulated fuel injector feed arm with sudden expansion/contraction, Fuel 186 (2016) 534–543. doi:10.1016/j.fuel.2016.08.080.

[5] C. Moses, G. Wilson, S. Byrnes, Effect of Red Dye Contamination on the Fouling Rate of Aircraft, in: 8 th International Conference on Stability and Handling of Liquid Fuels, Steamboat Springs, Colorado, 2003.

[6] C. Moses, G. Wilson, IASH 2007, the 10th International Conference on Stability, Handling and Use of Liquid Fuels Tucson, Arizona October 5-11, 2007, in: Studies of the Kinetics of Jet Fuel Thermal Stability By Laser Induced Fluorescence, 2007.

[7] J. L. Krazinski, S. P. Vanka, J. A. Pierce, W. M. Roquemore, A Computational Fluid Dynamics and Chemistry Model for Jet Fuel Thermal Stability, in: ASME-90-GT, 1990.

[8] W. M. Roquemore, K. V. Reddy, A Time Dependent Model with Global Chemistry for Decomposition and Deposition of Aircraft Fuels, in: Symposium on the Stability and Oxidation Chemistry of Middle Distillate Fuels, 1990, pp. 1346–1357.

[9] V. R. Katta, R. W. M, Numerical Method for Simulating Fluid-Dynamic and Heat Transfer Changes in Jet Engine Injector Feed Arm Due to Fouling, Journal of Thermophysics and Heat Transfer 7 (1993) 651–661.

[10] S. Zabarnick, Chemical Kinetic Modeling of Jet Fuel Autoxidation and Antioxidant Chemistry, Industrial & Engineering Chemistry Research 32 (1993) 1012–1017.

[11] S. Zabarnick, Pseudo-Detailed Chemical Kinetic Modeling of Antioxidant Chemistry for Jet Fuel Applications 0624 (97) (1998) 547–553.

[12] N. J. Kuprowicz, J. S. Ervin, S. Zabarnick, Modeling the liquid-phase oxidation of hydrocarbons over a range of temperatures and dissolved oxygen concentrations with pseudo-detailed chemical kinetics, Fuel 83 (13) (2004) 1795–1801. doi:10.1016/j.fuel.2004.03.013.

[13] H. W. Fink, Donald G.; Beaty, Standard Handbook for Electrical Engineers, McGraw-Hill, 2000.

[14] D. Boss, R. N. Hazlett, R. L. Shepard, Analysis of n-Paraffin Oxidation Products in the Presence of Hydroperoxides, Analytical chemistry 45 (14) (1973) 14–18.

[15] Z. J. West, S. Zabarnick, R. C. Striebich, Determination of Hydroperoxides in Jet Fuel via Reaction with Triphenylphosphine, Industrial & Engineering Chemistry Research 44 (10) (2005) 3377–3383. doi:10.1021/ie0490379.

[16] J. S. Ervin, S. Zabarnick, T. F. Williams, One-Dimensional Simulations of Jet Fuel Thermal-Oxidative Degradation and Deposit Formation Within Cylindrical, Journal of Energy Resources Technology 122 (December) (2000) 229–238. doi:10.1115/1.1326915.

[17] E. Alborzi, S. Blakey, H. Ghadbeigi, C. Pinna, M. Pourkashanian, C. Wilson, Analysis of the structure of deposited materials at inner surface of jet fuel injector feed arm with optical and scanning electron microscopy, in: 12 $^{\text{th}}$ International Conference on Stability and Handling of Liquid Fuels, Saratosa, Florida, 2011.

[18] T. Shuichi, W. J. Yangb, Thermal Transport in Turbulent Coutte Flows in Concentric Annuli for Various Prandtl Numbers, Numerical Heat Transfer, Part A: Applications: An International Journal of Computation and Methodology 34 (5) (1998) 537–552. doi:10.1080/10407789808914002.

[19] Margaret, Adamson. and Jamey, Tatro. and Margaret, Fiore. and Jessica, Fisher, Handbook of Aviation Fuel Properties, 4th Edition, Coordinating Research Council, Inc., 2014.

[20] Incropera, F P. and David, P Dewitt. and Theodore, L Bergman. and Adrienne, S Lavine , Introduction to Heat Transfer, 5th Edition, Wiley, 2002.

[21] A. S. Wade, A theoretical inverstigation into thermal oxidation and deposition processes in aviation fuels using genetic algorithms, Ph.D. thesis, University of Leeds (January 2005).

[22] R. Hooke, T. A. Jeeves, Direct Search" Solution of Numerical and Statistical Problems, Journal of the ACM 8 (2) (1961) 212–229. doi:http://dx.doi.org/10.1145/321062.321069.

[23] J. A. TeVelde, M. R. Glickstien, Heat Transfer and Thermal Stability of Alternative Aircraft Fuels, Tech. rep. (1983).